ELSEVIER

Journal of Luminescence 86 (2000) 375–382

JOURNAL OF LUMINESCENCE

www.elsevier.com/locate/jlumin

Signal correlator with programmable variable time delay based on optical coherent transients

K.D. Merkel*, Z. Cole, W.R. Babbitt

Physics Department, Montana State University, Bozeman, MT 59717-3840, USA

Abstract

An optical coherent transient signal correlator with variable true time delay is experimentally demonstrated. Storage of a pattern waveform in a spectral-spatial population grating is achieved by interfering it with two chirped pulses instead of a single brief reference pulse. Correlative signal processing results when a data waveform probes that grating, stimulating an emitted coherent output signal after the appropriate time delay. The signal is the result of a six-wave mixing process that can be as efficient as the traditional four-wave mixing process using a single brief reference pulse. Frequency shifting of the two chirped pulses enables programming of a variable time delay in the grating without changing the timing of the programming pulses. This concept is experimentally demonstrated with variable time delays over 448 ns (offset by greater than 1 μs) for the auto-correlation of a code with an experimentally limited bandwidth of 40 MHz. Processing bandwidths exceeding 10 GHz are achievable in materials such as Tm^{3+}:YAG (0.1 at%).

PACS: 42.79H; 42.50M; 42.65H; 42.40L

Keywords: Optical coherent transients; Correlation signal processing; Four-wave mixing; Six-wave mixing; Linear frequency chirped optical pulses

1. Introduction

In the operation of large broadband antenna arrays, a key issue is the efficient implementation of controllable, broadband true time delays [1]. Optical coherent transients (OCT) technology has an inherent capability of performing phase- and amplitude- sensitive processing on signals with bandwidths in excess of 10 GHz, while simultaneously imposing a variable true-time-delay of up to several microseconds on the result. Such features make OCT an extremely promising technology for future radar systems.

Here, an OCT variable time delay correlator device in a preferable configuration is described and experimentally demonstrated for the first time. A pattern waveform and variable true-time delay are programmed in the inhomogeneously broadened transition (IBT) by resonant interaction with absorbing atoms in a solid. This device utilizes an approach for an OCT signal processor [2–5] without brief pulses [6]. Two long, linear frequency chirped optical pulses are used in place of a traditional brief reference pulse (BRP), lowering the

* Corresponding author. Tel.: 406-994-7241.

E-mail address: merkel@spectrum.montana.edu (K.D. Merkel)

0022-2313/00/$ - see front matter
PII: S0022-2313(00)00181-2

instantaneous power requirements. The spectral-spatial population grating is therefore programmed into the optical sample by three (rather than two) temporally distinct and angled optical waveforms. In the configuration demonstrated here, the pattern waveform is applied first, followed by the chirped pulses, where the chirp rate of the first is twice that of the second. Once the grating is stored, the application of a data waveform causes the atoms in the interaction volume to emit a coherent optical signal representing the correlation of the pattern and data waveforms. Variable time delay signal processing is experimentally demonstrated by frequency shifting of the chirped programming pulses [7]. Although writing a grating with three such pulses and probing with one is effectively a six-wave mixing process, where one pulse acts to second order, the process can be highly efficient. The efficiency is discussed theoretically and demonstrated experimentally.

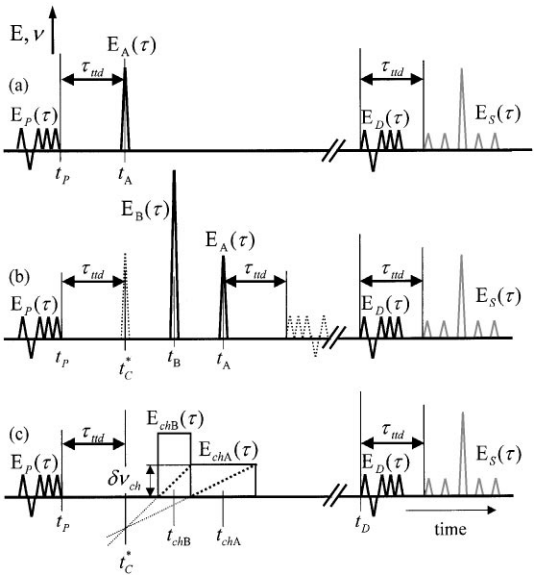

Fig. 1. Correlative signal processing using (a) traditional four-wave mixing with a single brief reference pulse, (b) six-wave mixing with two brief reference pulses, and (c) six-wave mixing with two chirped reference pulses.

2. Theory

2.1. Traditional OCT signal processing

Traditionally in OCT signal processing, a spectral-spatial holographic population grating is stored in an IBT by interfering a pattern waveform with a BRP [2]. By applying a data waveform to this grating at some later time, the medium emits a signal that represents the convolution or correlation of the pattern and the data pulses after a time delay. For the operation of correlation, as shown in Fig. 1(a), the pattern waveform $E_{\mathrm{P}}(\tau)$ is applied first. The time t_{P} marks the final edge of the pattern waveform. A BRP denoted as $E_{\mathrm{A}}(\tau)$ is next applied at time t_{A}, so that the stored time delay is measured as $\tau_{\mathrm{ttd}} = t_{\mathrm{A}} - t_{\mathrm{P}}$. In this traditional case, the pattern waveform excites some atoms in the absorbing material, depending on its frequency content, into a well-defined coherence state of the absorbers in the IBT. This coherence state dephases due to the inhomogeneous profile of resonant frequencies of the excited absorbers. The BRP acts to convert those dephased coherent atoms to a spectral population grating in the excited and ground states of the IBT. The BRP is most effective when it has a pulse area of $\pi/2$ in optically thin media, meaning that its power is sufficient to coherently excite half the atoms that are resonant with the optical carrier. The interference of the BRP with the dephasing atoms stores a spectral grating that contains information about the amplitude and phase of $E_{\mathrm{P}}(\tau)$, modulated by a periodic term containing τ_{ttd} , as described previously [2]. Applying $E_{\mathrm{D}}(\tau)$ to this grating at some later time stimulates rephasing towards a coherent response. The medium emits an output signal representing, in this case, the correlation of the pattern and data waveforms at a time τ_{ttd} after the beginning of $E_{\mathrm{D}}(\tau)$. This emitted signal is the result of coherent time-domain four-wave mixing, where two optical pulses write the grating, one pulse probes the grating, and one coherent output signal is emitted.

2.2. Six-wave mixing signal processing

Interestingly, the identical result can be obtained by a six-wave mixing process, (or, any higher-order

even-numbered wave mixing process). This process is depicted in Fig. 1(b), using brief pulses. While the process in Fig. 1(b) is not practical, it is an illuminating step towards the preferred process, as shown in Fig. 1(c). Fig. 1(b) shows an input pulse sequence where the pattern $E_P(\tau)$ is applied at time t_P, followed by $E_B(\tau)$, a BRP applied at t_B that ideally has pulse area π, meaning that its power is sufficient to invert the state of the atoms on resonance with the carrier. Thus, $E_P(\tau)$ establishes coherences among the absorbers in the IBT and $E_B(\tau)$ acts to invert the phase evolution of the atomic coherences after they have dephased up to t_B, corresponding to a dephasing time $(t_B - t_P)$, at which point they begin to rephase towards a photon echo of the pattern pulse. This rephasing event is shown as the dashed time-reversed replica of $E_P(\tau)$ mirrored around $E_B(\tau)$. Before the rephasing event occurs, a BRP $E_A(\tau)$ with area $\pi/2$ is applied at t_A. The effect of $E_A(A)$ is to convert the rephasing coherences to a population grating, where the stored time delay τ_{tdd} is now measured as the time between the replica of $E_P(\tau)$ and t_A. As a result of the condition $(t_B - t_P) > (t_A - t_B)$, the actual physical coherences are in a state of rephasing at the time the grating is written (contrary to Fig. 1(a) where they are dephasing) but rephasing in a phase-inverted, or time-reversed, manner. Thus, when $E_D(\tau)$ is applied to this grating, the emitted signal $E_S(\tau)$ represents the correlation of $E_P(\tau)$ and $E_D(\tau)$ delayed by τ_{ttd}, identical to the result in Fig. 1(a). This prediction is confirmed by numerical integration of the optical Bloch equations for a thin sample, neglecting the effects of non-reversible coherence loss processes. In both cases, the grating is written at time t_A, where $(t_A - t_P)$ is longer in Fig. 1(b).

Fig. 1(b) also shows a "virtual image" of $E_A(\tau)$ mirrored around $E_B(\tau)$ at time t_C^*, creating a conceptually convenient although nonphysical picture of the programming pulses acting as if time were running backwards, starting from t_A. In this time-reversed picture, pulses $E_A(\tau)$ and $E_B(\tau)$ act to create an image coherence at time t_C^*. This coherence can be thought of as the reference pulse used to store the pattern pulse $E_P(\tau)$. In this picture, the delay τ_{ttd} can also be measured as the time between t_C^* and t_P, or $\tau_{ttd} = t_C^* - t_P$.

2.3. OCT signal processing without brief pulses

From a systems perspective, the brief reference pulses in Fig. 1(a) and (b) are an impractical means for programming a spectral grating because of their relatively high power requirement that increases with the bandwidth squared. For example, in the current material of interest, Tm^{3+} : YAG (0.1 at%) for a bandwidth of approximately 30 GHz it takes $\sim 100\ GW/cm^2$ to coherently excite half the atoms in the IBT, an extremely high value that is on the order of the damage threshold of the optical sample. Rather, it is desirable to apply only low-power optical radiation to the absorbing medium and reduce the instantaneous power requirements of the system.

Two linear frequency chirped pulses can directly replace the brief pulses in Fig. 1(b), as shown in Fig. 1(c). The direct benefits, as noted previously, is that chirped pulses are of relatively low-power as compared to brief pulses [6], and allow one to achieve variable time-delay programming via frequency shifting [7].

Fig. 1(c) shows the preferred method for correlation using chirped pulses. The chirped pulses $E_{chB}(\tau)$ and $E_{chA}(\tau)$ have effective pulse areas π and $\pi/2$, arrival times t_{chB} and t_{chA}, durations τ_{chB} and τ_{chA}, and starting frequencies ν_{SB} and ν_{SA}, respectively. The chirp rate of $E_{chB}(\tau)$ is twice that of $E_{chA}(\tau)$ over the same chirp bandwidth $\delta\nu_{ch}$, so that $\tau_{chA} = 2\tau_{chB}$. In the figure, dashed lines represent the instantaneous frequency of the input pulses along the vertical axis.

As was the case for brief pulses in Fig. 1(b), $E_{chB}(\tau)$ inverts the dephasing coherences after the pattern pulse, and $E_{chA}(\tau)$ converts those coherences to populations. These physical mechanisms occur at different times for different frequencies within the IBT, rather than simultaneously as is the case when using BRPs. After the pattern pulse has been applied, there is never a rephasing of the coherences before $E_D(\tau)$ is applied, in direct contrast with the physical process that was demonstrated most recently in Ref. [7]. In that case, two chirped pulses are applied first to the sample, in the sequence $E_{chA}(\tau)$ and then $E_{chB}(\tau)$. These pulses prepare a coherence state in the medium that rephases and causes a photon echo to be emitted. Since this

photon echo extracts energy from the system [8], we can conjecture that the process depicted in Fig. 1(c) may be slightly more efficient than that demonstrated in Ref. [7], although this has not been experimentally demonstrated.

The net result of applying a pattern waveform and two chirped pulses is that the stored grating represents the pattern waveform and the time delay τ_{ttd}. The only difference between Fig. 1(b) and (c) is that, for a positive chirp rate, the higher frequencies experience more irreversible coherence loss than do the lower frequencies. Neglecting this factor, the output signal in Fig. 1(c) is identical to that in Fig. 1(a) and (b), namely the correlation of $E_p(\tau)$ and $E_D(\tau)$ emitted after τ_{ttd} .

When using the chirped reference pulses, it is now quite useful to examine the virtual timing relationships of the pulses. By extending the lines representing the chirp rates backward in time, these lines intersect at t_C^*, the time of the "virtual" image coherence as shown in Fig. 1(b). In this way, the stored time-delay τ_{ttd} can be easily referred to as $\tau_{ttd} = t_C^* - t_P$. Again, it should be noted that physically the grating at each frequency is not written until the application of $E_{chA}(\tau)$. In the time-reversed picture, this is the analog of producing a coherence (and photon echo) with two chirped pulses [7,9,10].

For this case of six-wave mixing, the output signal wave vector is given by the phase matching condition $\hat{k}_S = -\hat{k}_P + 2\hat{k}_{chB} - \hat{k}_{chA} + \hat{k}_D$. Several input beam scenarios are possible. The preferred case consists of one such set of input beam geometries, where perfect phase matching is met and each applied pulse has a different spatial direction. In such a scenario, the emitted signal would be detected in a spatial direction that is distinct from any of those used for the applied input pulses.

2.4. Efficiency considerations

The efficiency of both the four- and six-wave mixing processes, with either brief or chirped reference pulses, can be optimized by varying the power of the reference pulses. In this case we define the efficiency of the process as the power of the auto-correlation peak divided by the power in each bit of the pattern pulse and data pulse (not as a measure of the total energy out versus the total energy into the system. The energy in the chirped pulses is greater than for brief pulses, while the instantaneous power required in the brief pulses is higher than for the chirped pulses). In both simulations and in the experiment, the powers of the pattern and data pulses were fixed, so that the power of the auto-correlation peak is proportional to the strength of the grating. Simulations show that under optimized conditions, the efficiency of the four-wave and six-wave mixing processes are identical. When using chirped reference pulses, the efficiency is optimized and equal to the four-wave mixing process (as depicted in Fig. 1(a) with a single $\pi/2$ BRP) when the Rabi frequencies of the chirped pulses, Ω_{chA} and Ω_{chB}, for $E_{chA}(\tau)$ and $E_{chB}(\tau)$, respectively, are $\Omega_{chA} = 0.27\sqrt{\delta\nu_{ch}/\tau_{chA}}$ and $\Omega_{chB} \approx 3\Omega_{chA}$ for equal and fixed bandwidths for the pattern pulse, both chirped pulses and the data pulses. These results represent a range of time bandwidth products of the slow chirp $E_{chA}(\tau)$ from 20 to 640. When the pattern and data bandwidths are lower than the chirp bandwidth, then the ratio between chirped pulses is typically between three and four. In practice, the effects of propagation, absorption, coherence dephasing, and the use of Gaussian beams affects the optimization conditions; however, our experimental results, presented later in this paper, show the six- and four-wave mixing efficiencies to be within a factor of two. It is noteworthy that in the experiment, the ratio of the optimized chirped pulse Rabi frequencies is lower than that required in the simulation.

These simulation results for the Rabi frequencies of the chirped pulses can be used to estimate the savings in instantaneous power requirements when using the technique in Fig. 1(c) as compared to Fig. 1(a). Since the instantaneous power of the fast chirp approximately increases with $\delta\nu_{ch}/\tau_{chA}$ and of a BRP with $\delta\nu_{ch}^2$, then the ratio of these pulses is $\delta\nu_{ch}\tau_{chA}$, or the time bandwidth product of the slow chirp. For example, the instantaneous power of $E_{chB}(\tau)$ for a slow chirp over 10 GHz in 1 μs is four orders of magnitude lower than the instantaneous power required for $E_A(\tau)$ over the same bandwidth.

2.5. Variable time delays by frequency shifting

In addition to alleviating the problem of requiring high-power input signals, the use of chirped pulses allows for a simplified means of varying the time delay τ_{ttd} that is stored in the grating. In previously proposed OCT processors [2–5], the time delay could be varied only by externally generating a variation in the timing of the input pulses. Methods for varying the timing of the input pulses, such as imposing a variety of delay paths for signal propagation, are difficult to alter or adjust, consequently adding significant complications and cost to the system, and detracting from the benefits of optical signal processing. Frequency shifting of the chirped pulses [7] offers a convenient means of bypassing these complications.

Fig. 2 illustrates the concept of frequency shifting of the chirped pulses for the optimal case of correlation to achieve a variation in the time delay stored in the grating. This is done without changing the timing of the programming pulses. Fig. 2(b) duplicates Fig. 1(c), where $\nu_{SA} = \nu_{SB}$ and each chirp linearly ramps over $\delta\nu_{ch}$ from $(\nu_0 - \delta\nu_{ch}/2)/2)$ to $(\nu_0 + \delta\nu_{ch}/2)$, where ν_0 is the optical carrier frequency of the pattern and data waveforms.

By frequency shifting the two chirped pulses, the time t_C^* shown in Fig. 2(b) may be varied, altering the time delay τ_{ttd}. Defining the difference in the initial frequencies of the chirped pulses as $\delta\nu_{SBA} = \nu_{SB} - \nu_{SA}$, then $t_C^* = (2t_{chB} - t_{chA}) - \delta\nu_{SBA}(\tau_{chA}/\delta\nu_{ch})$. As $E_{chA}(\tau)$ acts to first order and E_{chB} acts to second order, a change in ν_{SA} (defined as $\delta\nu_{SA}$) has the same net result as an equal and opposite shift of ν_{SB}(defined as $\delta\nu_{SB}$). The frequency shifts effectively change the period of the spectral grating, thereby changing the "effective" time delay that each atom experiences without actually changing the timing $(t_{chB} - t_{chA})$. Using this technique, a variation in t_C^* with a fixed t_P translates to a change in τ_{ttd}.

The absolute value of the amount that the chirped pulses are frequency shifted with respect to each other, $\delta\nu_{SBA}$, should be less or equal to the difference between the chirped bandwidth $\delta\nu_{ch}$ for the pulses and the required processing bandwidth $\delta\nu_{proc}$. Typically, $\delta\nu_{proc}$ is defined by the bandwidth of the pattern pulse. The maximum delay tuning range by frequency shifting is $\pm(\delta\nu_{ch} - \delta\nu_{proc})(\tau_{chA}/\delta\nu_{ch})$. In a preferred embodiment, the chirped pulses can be frequency shifted by the same amount in opposite directions, such that $\delta\nu_{SA} = -\delta\nu_{SB}$, thereby maximizing the spectral overlap of the chirped pulses. For example, assuming a chirp rate of 10 GHz in 1 μs, then a shift of $\delta\nu_{SBA}$ of ± 100 kHz (± 1 GHz) corresponds to a time shift τ_{ttd} of ± 10 ps (± 100 ns) in the output signal $E_S(\tau)$. For an 8 GHz processor, 200 ns of delay tuning is possible with 10 ps delay resolution.

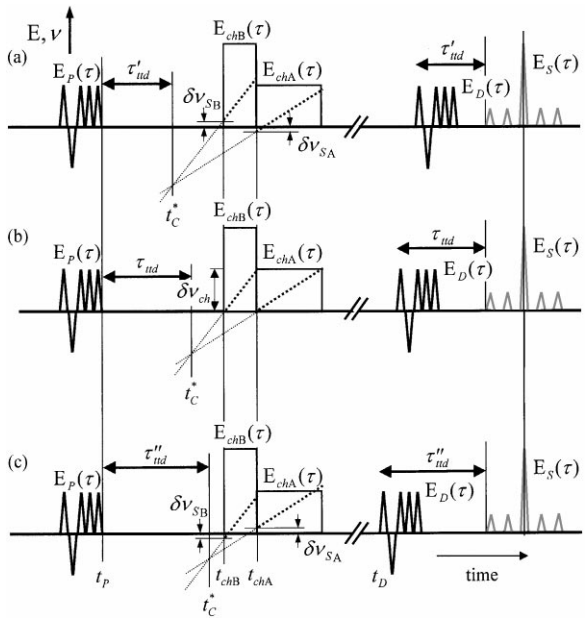

Fig. 2. Schematic of variable time delay correlation by frequency shifting without changing the timing of the programming pulses. The inputs in (b) have no change in the programmed time delay, while in (a) and (c) the time delays are made shorter and longer than in (b), respectively, by frequency shifting of the chirped pulses.

Fig. 2(a) shows the effect of a shorter stored delay τ'_{ttd} by frequency shifting in equal and opposite amounts so that $\delta\nu_{SBA} > 0$, without changing the input sequence timing. Since $\delta\nu_{SBA}$ is a positive value, t_C^* moves backward in time relative to Fig. 2(b), so that the value $(t_P - t_C^*)$ becomes shorter, which consequently decreases the time delay, τ'_{ttd}, relative to τ_{ttd}. Conversely, Fig. 2 (c) shows the effect of a longer stored delay τ''_{ttd} by equal and opposite values of $\delta\nu_{SA}$ and $\delta\nu_{SB}$ so that $\delta\nu_{SBA} < 0$.

Thus, t_C^* moves forward in time relative to Fig. 2(b), so that the value $(t_P - t_C^*)$ becomes longer, which consequently increases the time delay τ''_{ttd} relative to τ_{ttd}.

Although the data waveform $E_D(\tau)$ and the pattern waveform $E_P(\tau)$ are identical to each other in Figs. 1 and 2, generally these can be different, and $E_D(\tau)$ can be continuous [3,4]. Moreover, Figs. 1 and 2 show the two chirped pulses being temporally distinct from each other, for convenience purposes. In actuality, these chirps can actually be temporally overlapping, on different spatial beams, provided that there is a sufficient temporal separation between each instantaneous frequency of each chirp that includes the effects of frequency shifting. Likewise, the data waveform and the emitted signal can be temporally overlapping provided that they are spatially isolated from each other as a result of the input beam geometry.

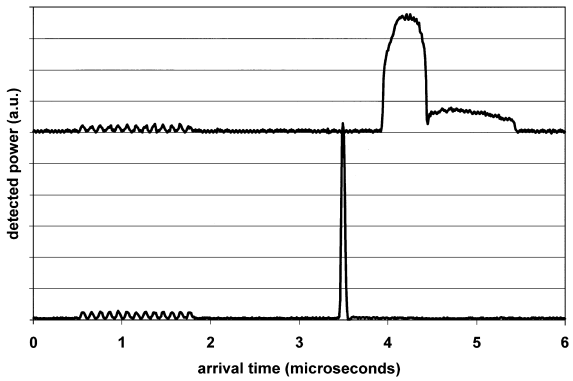

Fig. 3. Power of detected experimental input pulses used to demonstrate correlation signal processing by four-wave mixing using a single brief reference pulse (lower trace) and by six-wave mixing using two chirped reference pulses (upper trace). The vertical scale is the same in both traces.

3. Experimental Demonstrations

Experimental demonstrations of correlative signal processing were performed on the 793 nm transition [11] of Tm^{3+} in a YAG host crystal (0.1 at %) maintained at 5 K in a continuous flow liquid He coldfinger cryostat. The absorption coefficient was 2 cm^{-1}. The cw-output of a Ti : Sapphire laser was resonant with this transition and crafted into optical pulses by a 40 MHz acousto-optic modulator (AOM), driven by a 1 GHz arbitrary waveform generator. In all the experiments, the detected output signal was incident onto a silicon photodetector, and single shot events were captured on a 1.0 GHz digitizing oscilloscope.

3.1. Efficiency comparison experiment

To experimentally demonstrate the efficiency of the six-wave mixing process using chirped pulses, a linearly polarized optical beam was used, focused in a 200 μm spot ($1/e^2$ diameter) in a Tm^{3+} : YAG crystal that was 7 mm long, along a direction parallel to a single dipole orientation [12]. We measured a coherence time of approximately 20 μs.

Fig. 3 shows the input pulses that were used to experimentally compare the efficiencies of the four- and six-wave mixing processes. The lower trace shows the optimized input sequence for storing the pattern pulse with a brief reference pulse (mimicking Fig. 1(a)), while the top trace shows the input sequence for correlation using chirps (mimicking Fig. 1(c)). Both input sequences were designed to store the same time delay τ_{ttd}. In both cases, the pattern and data pulses were identical, being bi-phase 13-bit Barker codes, each bit being 50 ns on, 50 ns off, with peak powers of 10 mW. The brief reference pulse in the bottom trace was 50 ns in duration and optimized in power to be a $\pi/2$ pulse, via examination of the optical nutation signals, with a peak power of 350 mW. The two frequency chirped pulses had peak powers of 245 and 40 mW, durations of 0.5 and 1.0 μs, respectively, and were each chirped over 40 MHz. The power of the chirps was optimized to give the largest correlation signal, at a ratio of roughly 6 : 1, lower than that obtained by simulation.

Fig. 4 shows the experimental outputs that were obtained by directing the beam to a photodetector and using a gating AOM that turned on after the data pulse. A small portion of the data waveform that was scattered from the gating AOM can be seen in the background and serve as a reference for the timing of the emitted output signal. In the same style as in Fig. 3, the top trace is the result with chirped pulses, and the bottom trace is the result with a single brief reference pulse. The signal

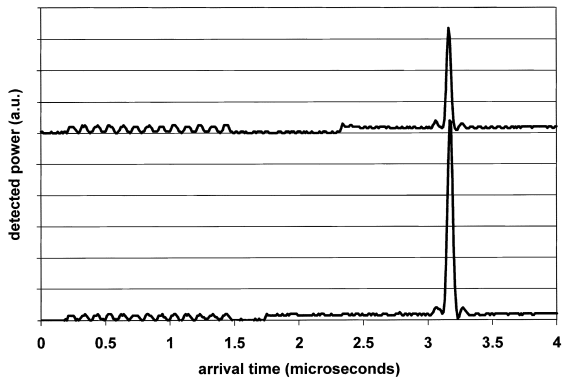

Fig. 4. Power of detected experimental output signals by four-wave mixing using a single brief reference pulse (lower trace) and by six-wave mixing process using two chirped reference pulses (upper trace). The vertical scale is the same in both traces.

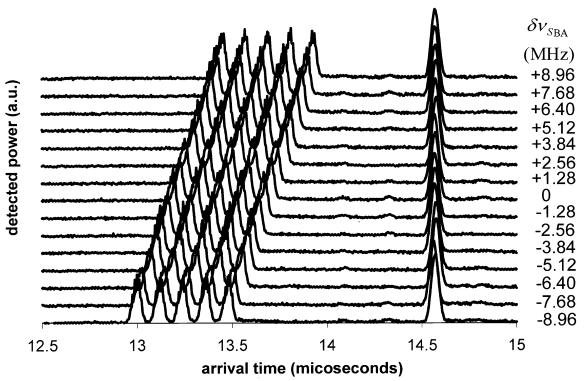

Fig. 5. Power of detected experimental correlation peaks (right) that are temporally aligned for applied data waveforms (left) with variable delays that were compensated for by varying $\delta\nu_{SBA}$ of the two chirped reference pulses before programming the spectral grating.

strength of the auto correlation peak using a single BRP was 3.50 mW, while the peak when using two chirped pulses is 1.85 mW. This result does not include the factor of the extra non-reversible coherence loss time of up to ~ 2 μs when using chirped reference pulses. These traces show that the efficiency of the four-wave mixing correlation process and six-wave mixing process are within a factor of two. The difference in efficiency is likely due to the effects of propagation, absorption, coherence dephasing, and the use of Gaussian beams.

3.2. Frequency-tuned variable time delay correlation experiment

Frequency-tuned variable time delay correlation signal processing was experimentally demonstrated in a non-single dipole Tm^{3+} : YAG crystal that was 5.5 mm long and maintained at 5K. In this experiment, the input pulses were directed towards the crystal along two beams, so that two additional identical AOM's deflected different portions of this pulse sequence onto either beam 1 or 2. These two beams were focussed and crossed in a 200 μm spot ($1/e^2$ diameter) in the crystal. The output beam was thus spatially isolated from the beam containing the data waveform, so that no gating AOM was needed after the sample.

In this case, the input sequence mimicked as shown schematically in Fig. 2. Both the pattern and data pulses were bi-phase 5-bit Barker codes, each bit being 50 ns on, 50 ns off, with peak powers of 45 mW. The two frequency chirped pulses, $E_{chB}(\tau)$ and $E_{chA}(\tau)$, had peak powers of 200 and 50 mW, durations of 0.5 and 1.0 μs, respectively, and were each chirped over 40 MHz. The pattern and π chirped pulse were on beam 1, and the π/2 chirped pulse and data were on beam 2. There was 1.6 μs between the pattern and π chirped pulse, and 320 ns between the two chirped pulses. For $\delta\nu_{SBA} = 0$, the data occurred 6.4 μs after the π/2 chirped pulse ended.

Fig. 5 shows the experimental results for 15 variations in the arrival time of data waveform (shown on the left) in 32 ns increments. These data waveforms simulate those in a true-time delay radar receiver processor, where a common data waveform arrives at each array element at a different time due to reception of an angled wavefront. An OCT frequency tuned delay on each element can compensate for the different arrival times while simultaneously correlating the waveforms with the stored pattern, resulting in temporally aligned emitted correlation peaks, as shown on the right of Fig. 5. In all cases, the programming pulse timing was fixed and equal and opposite changes were given to ν_{SB} and ν_{SA}. To produce each 32 ns timing increment, $\delta\nu_{SBA}$ was incremented by 1.28 MHz. Delays of $\pm$ 224 ns were achieved, offset by greater

than 1 μs. The emitted correlation peaks were detected along beam 1, and the maximum power of these signals was 0.6 mW. The data waveforms in Fig. 3 (left) were scattered from beam 2 ($\sim$1% scattering) to serve as timing references.

These results show an optimized correlation scheme for variable time delay processing. These captured waveforms are single-shot recordings, and the $\sim$1 ns timing jitter in the triggering electronics of the experiment are apparent in the data. However, the time-delay resolution of the OCT process has been documented at a level of < 75 ps RMS when using averaged output signals [13].

For the case of a non-persistent IBT, the concept of continuously programming of the grating could be employed [14]. Further, the demonstrated temporal processing capability could be combined with conventional Fourier optical processing techniques, so that coherently summing the output signals would greatly enhance the detection sensitivity, as in a phased array antenna.

4. Summary

In summary, we have demonstrated a technique for programming variable time delays of a pattern waveform in a spectral grating, without changing the timing of the programming pulse sequence. Two, long, low-power frequency chirped reference pulses are used in a six-wave mixing process that results in a signal correlator with variable time delay. This device has an efficiency comparable to the traditional four-wave mixing correlation process. Variable true-time delays over a 448 ns range were achieved. The demonstrated correlator bandwidth of 40 MHz only utilized $\sim$0.2% of the bandwidth available in Tm^{3+}:YAG (0.1 at%). This technique has the potential to allow versatile, all-optical reception and processing of >10 GHz signals in broadband array antenna beamforming.

Acknowledgements

We gratefully acknowledge the support for this work by the U.S. Army Research Office under the Defense Experimental Program to Stimulate Competitive Research, grant DAAG55-98-1-0244.

References

[1] T.C. Cheston, J. Frank, "Phased array radar antennas,", in: M.I. Skolnik (Ed.), Radar Handbook, McGraw-Hill, NY, 1992 Chapter 7.
[2] Y.S. Bai, W.R. Babbitt, N.W. Carlson, T.W. Mossberg, Appl. Phys. Lett. 45 (1984) 714.
[3] W.R. Babbitt, J.A. Bell, Appl. Opt. 33 (1994) 1538.
[4] M. Zhu, W.R. Babbitt, C.M. Jefferson, Opt. Lett. 20 (1995) 2514.
[5] X.A. Shen, Y.S. Bai, R. Kachru, Opt. Lett. 17 (1992) 1079.
[6] K.D. Merkel, W.R. Babbitt, Appl. Opt. 35 (1996) 278.
[7] K.D. Merkel, W.R. Babbitt, K.E. Anderson, K.H. Wagner, Opt. Lett. 24 (1999) 1386.
[8] C. Sjaarda Cornish, W.R. Babbitt, L. Tsang, unpublished.
[9] Y.S. Bai, T.W. Mossberg, Appl. Phys. Lett. 45 (1984) 1269.
[10] Y.S. Bai, T.W. Mossberg, Opt. Lett. 11 (1986) 30.
[11] R.M. Macfarlane, Opt. Lett. 18 (1993) 1958.
[12] Y. Sun, G.M. Wang, R.L. Cone, R.W. Equall, M.J.M. Leask, unpublished.
[13] K.D. Merkel, W.R. Babbitt, Opt. Lett. 23 (1998) 528.
[14] K.D. Merkel, W.R. Babbitt, Opt. Lett. 24 (1999) 172.